X-ray Structure of *fac*-IMn(CO)$_3$(bpy) and Electronic Structures and Transitions of the Complexes *fac*-XMn(CO)$_3$(bpy) (X = Cl, I) and *mer*-ClMn(CO)$_3$(bpy)

G. J. Stor,[†] D. J. Stufkens,*[,†] P. Vernooijs,[‡] E. J. Baerends,*[,‡] J. Fraanje,[§] and K. Goubitz[§]

Anorganisch Chemisch Laboratorium, Universiteit van Amsterdam, Nieuwe Achtergracht 166, 1018 WV Amsterdam, The Netherlands, Afdeling Theoretische Chemie, Vrije Universiteit, De Boelelaan 1083, 1081 HV Amsterdam, The Netherlands, and Laboratorium voor Kristallografie, Universiteit van Amsterdam, Nieuwe Achtergracht 166, 1018 WV Amsterdam, The Netherlands

Received August 6, 1993[⊗]

MO calculations have been performed on the complexes *fac*-XMn(CO)$_3$(bpy) (X = Cl, I) and *mer*-ClMn(CO)$_3$(bpy) in order to establish the influence of X on the electronic transitions of the *fac* and *mer* isomers and to interpret the differences in photochemical behavior of the *fac* and *mer* complexes. SCF calculations were performed with the Amsterdam density-functional program package ADF. The structural data used for the calculations were partly derived from the X-ray structure of *fac*-IMn(CO)$_3$(bpy) presented in the article. The theoretical data for the *fac* isomers show that the two highest occupied orbitals have metal-halide antibonding character and that the LUMO is a π^* (bpy) orbital. The first absorption band is therefore assigned to electronic transitions having mixed metal-halide to bpy CT character. The second absorption band is assigned to CT transitions from the corresponding metal-halide bonding orbitals to bpy. From a comparison of the theoretical and spectroscopic data, the intensities of these two absorption bands appear to depend on the metal character of the orbitals from which the electronic transitions originate. The main difference between the theoretical data of the *fac*- and *mer*-ClMn(CO)$_3$(bpy) complexes is the higher energy of the highest filled orbitals in the case of the *mer* isomer. This difference is in accordance with the spectroscopic data and may also explain the differences in photochemistry between the two isomers.

Introduction

The electronic structures and photochemical properties of the d^6 halide complexes M(CO)$_5$X (M = Mn, Re; X = Cl, Br, I) have received considerable attention.[1] Interestingly, the HOMO of these complexes appeared to have both metal d_π and halide p_π character, the halide p_π contribution increasing in the order Cl < Br < I at the expense of the metal d_π contribution. For all these complexes the primary photoprocess upon irradiation into the lowest-energy absorption band is loss of CO, although in some cases the net result of the photochemical reaction appeared to be M-X bond homolysis.[1q]

In the mid-1970s the related complexes *fac*-XRe(CO)$_3$(α-diimine) became of interest because of their ability to act as efficient photosensitizers[2] as well as catalysts in the reduction of CO_2.[3] With respect to the parent complexes Re(CO)$_5$X, these α-diimine compounds possess extra low-energy Re d → α-diimine π^* (MLCT) transitions.[2a,4] Irradiation into these transitions did not lead to a photoreaction. Only upon irradiation into the higher-energy transitions did the complexes show release of CO, just as the parent Re(CO)$_5$X compounds. The corresponding Mn complexes *fac*-XMn(CO)$_3$(α-diimine) were recently found to undergo a completely different and very remarkable photoreaction upon irradiation into their lowest-energy absorption band (Scheme 1).[5] An intriguing aspect of this reaction sequence is the difference in primary photoprocesses of the isomers *fac*- and *mer*-XMn(CO)$_3$(α-diimine). Whereas the *fac* isomers lose CO, the *mer* complexes undergo a Mn-X homolysis reaction. To our knowledge, this is the first example of such a homolysis reaction for this class of metal carbonyl halide complexes.

In this article, we present the results of MO calculations that have been performed on both isomers in order to understand this difference in photochemical behavior. In addition, the influence of the halide X on the composition of the molecular orbitals of *fac*-XMn(CO)$_3$(bpy) has been investigated and used for the assignment and characterization of their electronic

[†] Anorganisch Chemisch Laboratorium, Universiteit van Amsterdam.
[‡] Vrije Universiteit.
[§] Laboratorium voor Kristallografie, Universiteit van Amsterdam.
[⊗] Abstract published in *Advance ACS Abstracts,* February 15, 1995.

(1) (a) Gray, H. B.; Billig, E.; Wojcicki, A.; Farona, A. *Can. J. Chem.* **1963**, *61*, 1281. (b) Evans, S.; Green, J. C.; Green, M. L. H.; Orchard, A. F.; Turner, D. W. *Faraday Discuss. Chem. Soc.* **1969**, *47*, 112. (c) Fenske, R. F.; DeKock, R. L. *Inorg. Chem.* **1970**, *9*, 1053. (d) Blakney, G. B.; Allen, W. F. *Inorg. Chem.* **1971**, *10*, 2763. (e) Bamford, C. H.; Burley, J. W.; Coldbeck, M. *J. Chem. Soc., Dalton Trans.* **1972**, 1846. (f) Brown, T. L.; Berry, A. *Inorg. Chem.* **1972**, *11*, 1165. (g) Lichtenberger, D. L.; Sarapu, A. C.; Fenske, R. F. *Inorg. Chem.* **1973**, *12*, 702. (h) MacLean, R. A. N. *J. Chem. Soc., Dalton Trans.* **1974**, 1568. (i) Ceasar, G. P.; Milazzo, P.; Cikonski, J. L.; Levenson, R. A. *Inorg. Chem.* **1974**, *13*, 3035. (j) Hall, M. B. *J. Am. Chem. Soc.* **1975**, *97*, 2057. (k) Higginson, B. R.; Lloyd, D. R.; Evans, S.; Orchard, A. F. *J. Chem. Soc., Faraday Trans. 2* **1975**, *71*, 1913. (l) Allen, D. M.; Cox, A.; Kemp, T. J.; Sultana, Q.; Pitts, R. B. *J. Chem. Soc., Dalton Trans.* **1976**, 1189. (m) Wrighton, M. S.; Morse, D. L.; Gray, H. B.; Ottesen, D. K. *J. Am. Chem. Soc.* **1976**, *98*, 1111. (n) DeKock, R. L. In *Electron Spectroscopy: Theory, Techniques and Applications*; Brundle, C. R., Baker, A. D., Eds.; Academic Press: London, 1977; Vol. 1, Chapter 6, p 294. (o) Tyler, D. R.; Petrylak, D. P. *Inorg. Chim. Acta* **1981**, *53*, L185. (p) Jolly, W. L. *J. Phys. Chem.* **1983**, *87*, 26. (q) Pan, X.; Philbin, C. E.; Castellani, M. P.; Tyler, D. R. *Inorg. Chem.* **1988**, *27*, 671.

(2) See for example: (a) Wrighton, M. S.; Morse, D. L. *J. Am. Chem. Soc.* **1974**, *96*, 998. (b) Luong, J. C.; Nadjo, L.; Wrighton, M. S. *J. Am. Chem. Soc.* **1978**, *100*, 5790. (c) Stufkens, D. J. *Comments Inorg. Chem.* **1992**, *13*, 359 and references therein.

(3) (a) Hawecker, J.; Lehn, J. M.; Ziessel, R. *J. Chem. Soc., Chem. Commun.* **1984**, 328. (b) Sullivan, B. P.; Bolinger, M. C.; Conrad, D.; Vining, W. J.; Meyer, T. J. *J. Chem. Soc., Chem. Commun.* **1985**, 1414. (c) Hawecker, J.; Lehn, J. M.; Ziessel, R. *Helv. Chim. Acta* **1986**, *69*, 1990. (d) Breikss, A. J.; Abruña, H. D. *J. Electroanal. Chem. Interfacial Electrochem.* **1986**, *201*, 353.

(4) Geoffroy, G. L.; Wrighton, M. S. *Organometallic Photochemistry*; Academic Press: New York, 1979.

(5) Stor, G. J.; Morrison, S. L.; Stufkens, D. J.; Oskam, A. *Organometallics* **1994**, *13*, 2641.

0020-1669/95/1334-1588$09.00/0

Scheme 1

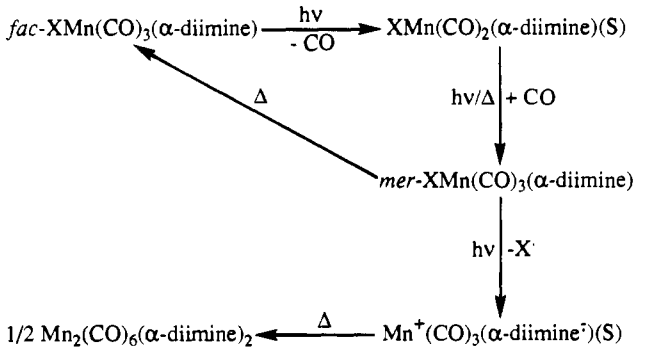

Table 1. CO Stretching Frequencies and Experimental and Calculated Energies of the Low-Energy Transitions (ΔE_{max}) of the $XMn(CO)_3$(bpy) Complexes in THF at Room Temperature

complex	ν(CO)/cm^{-1}	ΔE_{max} (exp)/eV	ΔE_{max} (calc)[a]/eV
fac-$ClMn(CO)_3$(bpy)	2025 s, 1936 m, 1913 m	2.95, 3.45	2.31, 3.55 (1.39, 2.43)
fac-$BrMn(CO)_3$(bpy)	2023 s, 1935 m, 1914 m	2.89, 3.32	
fac-$IMn(CO)_3$(bpy)	2019, s, 1933 m, 1916 m	2.79, 3.23	(1.17, 2.15)
mer-$ClMn(CO)_3$(bpy)			(1.09, 2.44)
mer-$BrMn(CO)_3$(bpy)	2043 vw, 1948 s, 1903 m	2.44, 3.32	

[a] Values in parentheses defined as orbital energy differences.

transitions. The bond distances used for these MO calculations were partly derived from the crystal structure data for *fac*-$IMn(CO)_3$(bpy), which are also reported in this article.

Experimental Section

Preparations. The complexes *fac*-$XMn(CO)_3$(bpy) (X = Cl, Br, I) were synthesized as previously described.[6] Their IR and UV/vis data are summarized in Table 1. The complexes *mer*-$XMn(CO)_3$(bpy), intermediates in the reaction of Scheme 1, could not be isolated due to their thermal instability above 213 K. Their meridional structure was evident from the typical frequency and intensity pattern of the IR CO bands (Table 1) and further established by force field calculations.[5] The complexes are air stable but photodecompose upon exposure to visible light.

Spectroscopic Measurements. IR spectra were measured on a Nicolet 7199B FTIR interferometer provided with a liquid-nitrogen-cooled MCT detector (32 scans, resolution 1.0 cm^{-1}). Electronic absorption spectra were recorded on a Perkin-Elmer Lambda 5 UV/vis spectrophotometer, which was connected to a 3600 data station.

MO Calculations. The calculations reported in this paper have been performed with the Amsterdam density-functional program package ADF.[7,8] The computational scheme is characterized by the use of a density-fitting procedure to obtain accurate Coulomb and exchange-correlation potentials in each SCF cycle, by accurate and efficient numerical integration[9] of the Hamiltonian matrix elements and by the possibility to freeze core orbitals. The effective one-electron Hamiltonian was based on the local density approximation (LDA) to the exact Kohn–Sham[10] exchange-correlation potential. The LDA derives the potential at position **r** from the homogeneous electron gas, with density equal to the local electron density $\varrho(\mathbf{r})$ in the molecule. For the exchange potential, this yields the familiar Slater $\varrho^{1/3}$ potential,[11] and for the correlation potential, the Vosko–Wilk–Nusair parametrization[12] of the homogeneous electron gas correlation energies has been used.

Table 2. Crystallographic Data and Refinement Details for *fac*-$IMn(CO)_3$(bpy)

chem formula	$C_{13}H_8N_2O_3MnI$	V/Å^3	701.3(2)
M_r	422.1	Z	2
crystal class	triclinic	D_x/g·cm^{-3}	2.0
space group	$P\bar{1}$	λ(Cu Kα)/Å	1.5418
a/Å	6.9993(9)	μ(Cu Kα)/cm^{-1}	252.8
b/Å	10.006(1)	F(000)	404
c/Å	10.545(1)	T/K	293
α/deg	83.11(2)	R	0.098
β/deg	80.25(1)	R_w	0.119
γ/deg	75.16(1)		

The molecular orbitals were expanded in an uncontracted double-ζ STO basis set for all atoms, with the exception of the transition metal orbitals, for which we used a triple-ζ STO *n*d basis set, double-ζ (n + 1)s and single-ζ (n + 1)p. On H, Cl, Br, and I we added one polarization function (2p, 3d, 4d, and 5d, respectively). The cores (Mn, Cl 1s–2p; Br 1s–3p; I 1s–4p; C, N 1s) have been kept frozen.

In order to analyze the metal–ligand interaction energies and the composition of the orbitals, we used the fragments CO and bipyridine, the atom Mn, and the halide X. This means that the MO's are expanded in the converged molecular or atomic orbitals of these fragments. The Mulliken gross population of a fragment orbital (FO) in a molecular orbital is used to denote the percentage FO character of that molecular orbital. As a first approximation to excitation energies, the differences between one-electron energies of the appropriate virtual and occupied molecular orbitals may be used. This is a better approximation in density-functional calculations than in Hartree–Fock calculations, since the former do not suffer from the well-known artifact of Hartree–Fock calculations of putting the virtual levels too high by having the virtual electrons move in the field of N instead of N − 1 electrons. Since, however, these one-electron energy differences yield rather too low excitation energies compared to experiment, we have explicitly performed separate SCF calculations of the excited states in one case, viz. *fac*-$ClMn(CO)_3$(bpy).

Crystal Structure Determination of *fac*-$IMn(CO)_3$(bpy). The experimental details of the crystal structure determination of *fac*-$IMn(CO)_3$(bpy) are collected in Table 2. A crystal with dimensions 0.05 × 0.50 × 0.88 mm approximately was used for data collection on an Enraf-Nonius CAD-4 diffractometer with graphite-monochromated Cu Kα radiation and a θ–2θ scan. A total of 2877 unique reflections were measured within the range $0 \le h < 8$, $-11 \le k \le 12$, $-12 \le l \le 13$. Of these, 2765 were above the significance level of $2.5\sigma(I)$. The maximum value of (sin θ)/λ was 0.63 Å^{-1}. Unit-cell parameters were refined by a least-squares fitting procedure, using 23 reflections with $80° \le 2\theta \le 90°$. Corrections for Lorentz and polarization effects were applied. The Mn and I positions were found by direct methods, using the program SIMPEL.[13] The remainder of the non-hydrogen atoms were found in a subsequent ΔF synthesis. The hydrogen atoms were calculated. Block-diagonal least-squares refinement on F, with anisotropic thermal parameters for the non-hydrogen atoms and by keeping the hydrogen atoms fixed on their calculated positions with U = 0.08 Å^2, converged to R = 0.098, R_w = 0.119, and $(\Delta/\sigma)_{max}$ = 0.78. A weighting scheme $w = (4.1 + F_o + 0.009(F_o)^2)^{-1}$ was used. An empirical absorption correction (DIFABS)[14] was applied, with coefficients in the range 0.51–1.97. A final difference Fourier map revealed a residual electron density between −3.8 and 5.2 e Å^{-3}. Scattering factors were taken from Cromer and Mann.[15] The anomalous scattering of Mn and I was taken into account. All calculations were performed with XTAL,[16] unless stated otherwise. The fractional coordinates and the equivalent isotropic thermal parameters of the non-hydrogen atoms are given in Table 3, and the bond distances and angles for the non-hydrogen atoms are given in Table 4.

(6) Staal, L. H.; Oskam, A.; Vrieze, K. *J. Organomet. Chem.* **1979**, *170*, 235.
(7) Baerends, E. J.; Ellis, D. E.; Ros, P. *Chem. Phys.* **1973**, *2*, 52.
(8) Baerends, E. J.; Ros, P. *Int. J. Quantum. Chem.* **1978**, *S12*, 169.
(9) te Velde, G.; Baerends, E. J. *J. Comput. Phys.* **1992**, *99*, 84.
(10) Kohn, W.; Sham, L. J. *Phys. Rev.* **1965**, *A140*, 1133.
(11) Slater, J. C. *Quantum Theory of Molecules and Solids*; McGraw-Hill: New York, 1974; Vol. 4.
(12) Vosko, S. H.; Wilk, L.; Nusair, M. *Can. J. Phys.* **1980**, *58*, 1200.
(13) Schenk, H.; Hall, S. R. In *SIMPEL XTAL2.6 User's Manual*; Hall, S. R., Stewart, J. M., Eds.; Universities of Western Australia and Maryland, 1989.
(14) Walker, N.; Stewart, D. *Acta Crystallogr., Sect. A: Found Crystallogr.* **1983**, *A39*, 158.
(15) (a) Cromer, D. T.; Mann, J. B. *Acta Crystallogr., Sect. A: Cryst. Phys. Diffr. Theor. Gen. Crystallogr.* **1968**, *A24*, 321. (b) Cromer, D. T.; Mann, J. B. *International Tables for X-Ray Crystallography*; Kynoch Press: Birmingham, England, 1974, Vol. IV; p 55.
(16) Hall, S. R.; Stewart, J. M., Eds. *XTAL2.6 User's Manual*; Universities of Western Australia and Maryland, 1989.

Table 3. Fractional Coordinates and Equivalent Isotropic Thermal Parameters for the Non-Hydrogen Atoms of *fac*-IMn(CO)$_3$(bpy) with Esd's in Parentheses

atom	x	y	z	U_{eq}/Å^2
I	0.6894(1)	0.1629(1)	0.24874(9)	0.0238(6)
Mn	0.2949(3)	0.2820(2)	0.3185(2)	0.016(1)
C(1)	0.247(2)	0.209(2)	0.070(1)	0.019(7)
C(2)	0.241(2)	0.217(2)	−0.062(1)	0.025(8)
C(3)	0.244(3)	0.340(2)	−0.134(1)	0.034(9)
C(4)	0.260(2)	0.452(2)	−0.076(1)	0.029(8)
C(5)	0.274(2)	0.437(2)	0.055(1)	0.024(8)
C(6)	0.237(2)	0.083(2)	0.158(1)	0.019(7)
C(7)	0.219(3)	−0.040(2)	0.119(2)	0.028(8)
C(8)	0.197(3)	−0.146(2)	0.210(2)	0.04(1)
C(9)	0.200(3)	−0.131(2)	0.339(2)	0.03(1)
C(10)	0.221(2)	−0.005(2)	0.370(2)	0.025(8)
C(11)	0.318(2)	0.232(2)	0.483(1)	0.025(8)
C(12)	0.371(2)	0.438(2)	0.333(1)	0.021(7)
C(13)	0.039(2)	0.370(2)	0.367(1)	0.024(8)
N(1)	0.270(2)	0.317(1)	0.126(1)	0.020(6)
N(2)	0.241(2)	0.101(1)	0.284(1)	0.021(6)
O(11)	0.340(2)	0.205(2)	0.593(1)	0.042(8)
O(12)	0.414(2)	0.538(1)	0.344(1)	0.035(7)
O(13)	−0.120(2)	0.434(1)	0.401(1)	0.040(7)

Table 4. Bond Distances (Å) and Angles (deg) for *fac*-IMn(CO)$_3$(bpy) with Esd's in Parentheses

Mn−I	2.724(2)	C(1)−N(1)	1.34(2)
Mn−C(11)	1.77(2)	C(2)−C(3)	1.37(3)
Mn−C(12)	1.80(2)	C(3)−C(4)	1.37(3)
Mn−C(13)	1.80(1)	C(4)−C(5)	1.39(2)
Mn−N(1)	2.05(1)	C(5)−N(1)	1.34(2)
Mn−N(2)	2.03(2)	C(6)−C(7)	1.38(3)
C(11)−O(11)	1.19(2)	C(6)−N(2)	1.37(2)
C(12)−O(12)	1.14(2)	C(7)−C(8)	1.37(2)
C(13)−O(13)	1.15(2)	C(8)−C(9)	1.39(3)
C(1)−C(2)	1.39(2)	C(9)−C(10)	1.38(3)
C(1)−C(6)	1.48(2)	C(10)−N(2)	1.33(2)
I−Mn−C(11)	90.6(5)	C(13)−Mn−N(1)	93.3(6)
I−Mn−C(12)	86.6(5)	C(13)−Mn−N(2)	96.8(7)
I−Mn−C(13)	176.3(6)	N(1)−Mn−N(2)	79.0(5)
I−Mn−N(1)	87.7(3)	C(1)−N(1)−C(5)	120(1)
I−Mn−N(2)	86.9(3)	C(1)−C(2)−C(3)	119(2)
Mn−C(11)−O(11)	176(2)	C(1)−C(6)−C(7)	124(1)
Mn−C(12)−O(12)	178(1)	C(1)−C(6)−N(2)	113(1)
Mn−C(13)−O(13)	176(2)	C(2)−C(1)−N(1)	121(1)
Mn−N(1)−C(1)	115.6(9)	C(2)−C(3)−C(4)	120(1)
Mn−N(1)−C(5)	125(1)	C(2)−C(1)−C(6)	123(2)
Mn−N(2)−C(6)	116(1)	C(3)−C(4)−C(5)	119(2)
Mn−N(2)−C(10)	127(1)	C(4)−C(5)−N(1)	121(2)
C(11)−Mn−C(12)	88.9(8)	C(6)−N(2)−C(10)	117(2)
C(11)−Mn−C(13)	88.8(7)	C(6)−C(7)−C(8)	119(2)
C(11)−Mn−N(1)	173.6(7)	C(6)−C(1)−N(1)	115(1)
C(11)−Mn−N(2)	94.8(7)	C(7)−C(6)−N(2)	122(1)
C(12)−Mn−C(13)	89.7(8)	C(7)−C(8)−C(9)	120(2)
C(12)−Mn−N(1)	97.1(6)	C(8)−C(9)−C(10)	118(2)
C(12)−Mn−N(2)	172.6(5)	C(9)−C(10)−N(2)	124(2)

Results and Discussion

Molecular Structure of *fac*-IMn(CO)$_3$(bpy). The structure of *fac*-IMn(CO)$_3$(bpy) is presented in Figure 1. The complex has C_s symmetry, with the atoms I and Mn and the axial CO ligand lying in the plane of symmetry. The coordination around the central Mn atom is nearly octahedral. The structural data agree with those for the related complexes *fac*-ClMn(CO)$_3$(Ph,-Me-DAB)[17] (DAB = 1,4-diaza-1,3-butadiene), *fac*-BrMn(CO)$_3$-(cHex-DAB),[18] and *fac*-ClRe(CO)$_3$(iPr-DAB).[19]

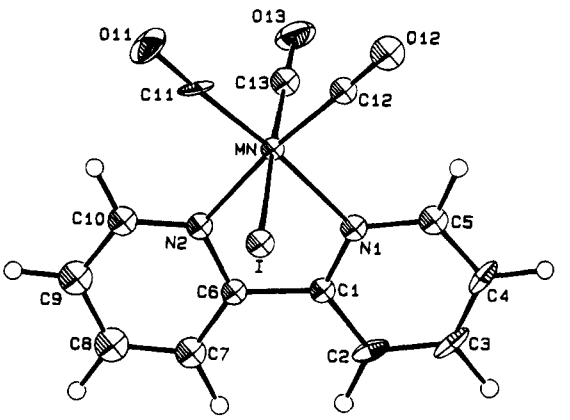

Figure 1. Crystal structure (ORTEP drawing) of *fac*-IMn(CO)$_3$(bpy).

Theoretical Analysis. MO calculations were performed on the complexes *fac*-XMn(CO)$_3$(bpy) (X = Cl, I) and *mer*-ClMn-(CO)$_3$(bpy).

The MO diagrams of *fac*-ClMn(CO)$_3$(bpy) and *fac*-IMn(CO)$_3$-(bpy) are presented in Figure 2, and the composition of the MO's is given in the Table 5. The LUMO 33a′ and the two following empty MO's 34a′ and 24a″ have 90% or more bpy π^* character. Instead of a single HOMO, there are two close-lying highest occupied orbitals 23a″ and 32a′, which give rise to one degenerate e orbital in the parent complexes Mn(CO)$_5$X.[1k,p] Both MO's are a combination of halide p and manganese d orbitals, which have an antibonding π interaction. Their bonding counterparts, 22a″ and 30a′ for X = Cl and 22a″ and 31a′ in the case of X = I are about 1 eV lower in energy. Both 23a″ and 32a′ have a high halide p contribution, which increases from about 60% for X = Cl to ca. 85% in the case of the iodide complex.

This result is rather amazing in view of the theoretical and UV-photoelectron (PE) data of the parent Mn(CO)$_5$X complexes. Although there has been some controversy about the level ordering of these latter complexes,[1a−d,g−i,k,n,p] the most recent PE spectra obtained by He I and He II excitation point to an energy ordering e(Mn) > b_2(Mn) > e(X) > a_1(Mn−X) in the case of X = Cl and Br and e(X) > b_2(Mn) > e(Mn) > a_1-(Mn−X) for X = I.[1k] This assignment was confirmed by calculations of Jolly, who used core binding energy data to correct valence ionization potentials for the effects of potential and relaxation energy.[1p] Substitution of two electron-withdrawing carbonyls by an electron-releasing α-diimine ligand such as bpy will cause a shift of the highest filled molecular orbital to higher energy and increase its metal character. This is e.g. evident from the PE spectra of Re(CO)$_5$Cl[20] and *fac*-ClRe(CO)$_3$-(iPr-DAB)[21] (DAB = 1,4-diaza-1,3-butadiene), which show a shift of the first ionization band from 8.8 to 7.76 eV upon replacement of the carbonyls by iPr-DAB. The high intensity of this band in the He II PE spectra confirms the strong metal character of these highest filled MO's. The bonding counterparts 22a″ and 30a′ (31a′ for X = I) have a rather high metal contribution (Table 5). Again this behavior is not reflected in the PE spectra of *fac*-ClRe(CO)$_3$(iPr-DAB), which show the ionizations from these orbitals as a rather weak band in the He II spectra.[21] Although we must of course be cautious with the extrapolation of these experimental PE data of *fac*-ClRe(CO)$_3$-(iPr-DAB) to the theoretical results obtained for *fac*-XMn(CO)$_3$-

(17) Schmidt, G.; Paulus, H.; van Eldik, R.; Elias, H. *Inorg. Chem.* **1988**, *27*, 3211.
(18) Graham, A. J.; Akrigg, B.; Sheldrick, B. *Cryst. Struct. Commun.* **1977**, *6*, 571.
(19) Graham, A. J.; Akrigg, B.; Sheldrick, B. *Cryst. Struct. Commun.* **1977**, *6*, 577.
(20) Cowley, A. H. *Prog. Inorg. Chem.* **1979**, *26*, 46.
(21) Andréa, R. R.; Louwen, J. N.; Kokkes, M. W.; Stufkens, D. J.; Oskam, A. *J. Organomet. Chem.* **1985**, *281*, 273.

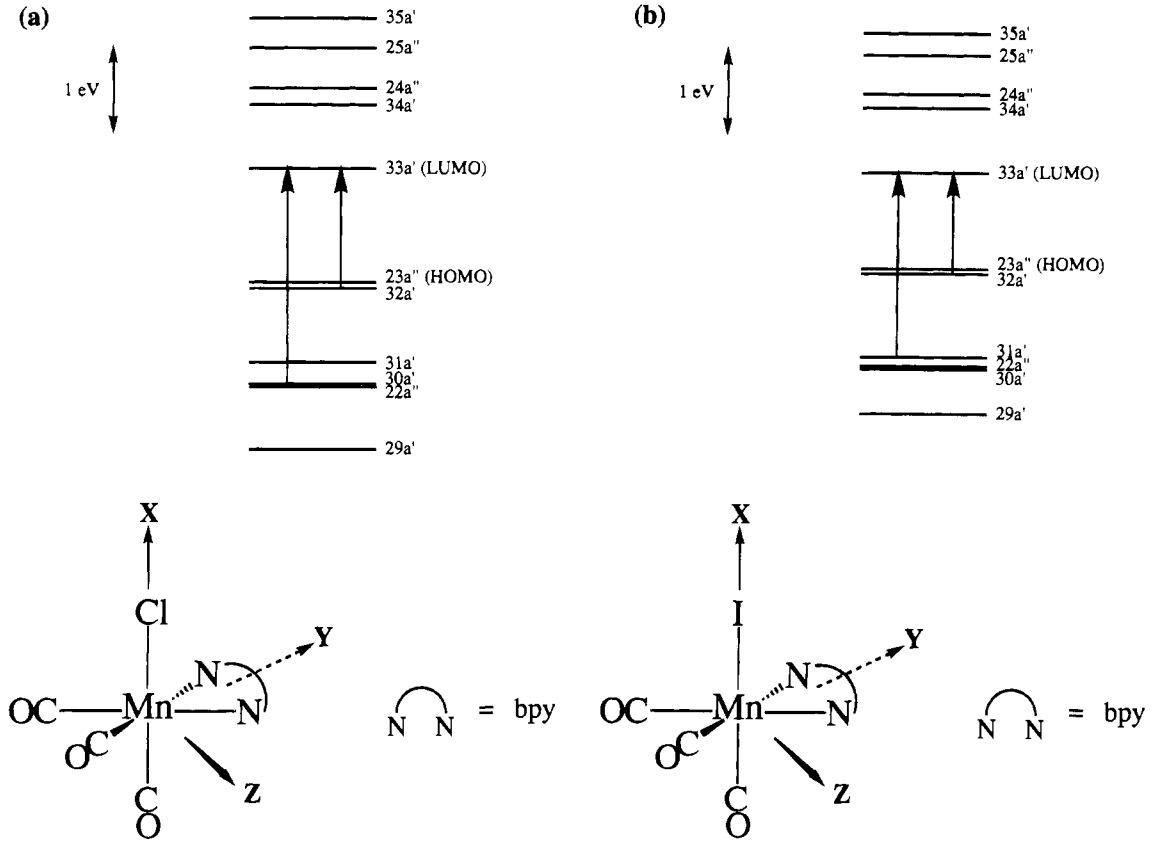

Figure 2. Relevant parts of the MO diagrams of *fac*-ClMn(CO)$_3$(bpy) (a) and *fac*-IMn(CO)$_3$(bpy) (b).

(bpy), our theoretical data still seem to overemphasize the halide character of the highest filled molecular orbitals. It will be shown hereafter that the assignment of the visible absorption bands of these *fac*-XMn(CO)$_3$(bpy) complexes leads to the same conclusion.

Orbital 31a′ (X = Cl) or 30a′ (X = I) is found at almost the same energy as the metal−halide π-bonding orbitals, and it is composed of Mn d_{z^2}, Mn $d_{x^2-y^2}$, and π^* orbitals of the equatorial CO ligands. The interactions between the metal d and CO π^* orbitals are all bonding.

About 1 eV below this group of three orbitals is situated 29a′, which has a large amount of halide p_x character (61% for X = Cl, 43% for X = I) and in addition some Mn $d_{x^2-y^2}$ (7% for X = Cl, 9% for X = I) and Mn p_x (7% for X = Cl, 8% for X = I) character. The interaction between these orbitals is strongly σ bonding. The antibonding counterpart of 29a′ is orbital 35a′, which is about 2 eV above the bpy π^* LUMO orbital 33a′. Just below 35a′ is situated orbital 25a″, which is mainly σ antibonding between Mn and bpy.

The MO level scheme of *mer*-ClMn(CO)$_3$(bpy) is presented in Figure 3 and Table 6. Although the molecular orbital ordering is the same as for the *fac*-isomer, the two highest occupied orbitals of the *mer* isomer (54 and 55) are about 0.3 eV higher in energy than the corresponding orbitals (32a′ and 23a″) of the *fac* isomer. The structural change also has a large influence on the composition of the orbitals. The Cl p_π orbitals are now $3p_x$ and $(1/2^{1/2})(3p_y + 3p_z)$. These interact in a π-antibonding manner with the Mn−Cl d_π orbitals $(1/2^{1/2})(d_{xz} - d_{xy})$ and $(3^{1/2}/2)d_{z^2} + (1/2)d_{x^2-y^2}$), respectively, to form the highest occupied orbitals 54 and 55. Since the HOMO (55) has predominantly d_{z^2} instead of d_{xz} (23a″) character, the dipole-allowed MLCT transition from this orbital to the lowest π^* orbital of bpy (56) is expected to have a low intensity because of small overlap between the orbitals.

Electronic Transitions and Photochemistry. The low-temperature absorption spectra of *fac*-XMn(CO)$_3$(bpy) (X = Cl, Br, I) are presented in Figure 4. They are characterized by two rather strong bands, the relative intensities of which depend on X. In previous studies, the lowest-energy band of these complexes[6] and of the corresponding Re ones[2a,4] has been assigned to MLCT transitions to the lowest π^* orbital of bpy. This assignment was based on the high intensity of the band, its solvatochromism, and the ligand dependence of its position. Quite recently, a resonance Raman (rR) study of *fac*-BrRe(CO$_3$-(pTol-DAB) showed that excitation into the lowest-energy band gives rise to a strong *rR* effect for ν(Re−Br).[22] This means that this transition is not purely MLCT in character but that especially the metal−halide bond is strongly affected. This conclusion is in accordance with the results from the MO calculations of these *fac*-XMn(CO)$_3$(bpy) complexes (Figure 2 and Table 5), which show that the lowest-energy transitions take place from the metal−halide antibonding orbitals 32a′ and 23a″ to the lowest π^* orbital of bpy, 33a′. From these transitions only 32a′ → 33a′ will be intense, since 32a′ contains Mn d_{xy} which strongly interacts with 33a′, the lowest π^* orbital of bpy (π-back-bonding). Orbital 32a′ is an antibonding combination of Mn d_{xy} and X p_y, and since X p_y has a much smaller overlap with 33a′, the intensity of the 32a′ → 33a′ transition will mainly be determined by the contribution of Mn d_{xy} to 32a′. The second transition 23a″ → 33a′ will be weak, since there is hardly any overlap between the orbitals (Mn d_{xz}, X p_z, and bpy π^*) involved in this transition. The same holds even more for the transition from 31a′ (X = Cl) or 30a′ (X = I) to 33a′.

According to the MO diagrams (Figure 2), the second absorption band may belong to transitions either from the highest filled orbitals 32a′ and 23a″ to the second π^* orbital of bpy (34a′) or from the orbitals 30a′ (X = Cl) or 31a′ (X = I) and

(22) Stor, G. J.; Stufkens, D. J.; Oskam, A. *Inorg. Chem.* **1992**, *31*, 1318.

Table 5. Characters and Energies of the MO's of *fac*-ClMn(CO)$_3$(bpy) and *fac*-IMn(CO)$_3$(bpy)

orbital	character	overlap factor	energy/eV
	(a) *fac*-ClMn(CO)$_3$bpy)		
	Unoccupied Orbitals		
35a′	34% Mn $d_{x^2-y^2}$ − 14% Cl p_x antibonding	0.082	−2.49
	4% Mn p_x − 14% Cl p_x antibonding	0.293	
25a″	33% Mn d_{yz} − 12% bpy σ antibonding	0.165	−2.83
	6% Mn p_z − 12% bpy σ antibonding	−0.302	
24a″	95% bpy π^*		−3.30
34a′	96% bpy π^*		−3.51
33a′	90% bpy π^*		−4.25
	Occupied Orbitals		
23a″	28% Mn d_{xz} − 59% Cl p_z antibonding	−0.075	−5.55
32a′	24% Mn d_{xy} − 62% Cl p_y antibonding	−0.075	−5.64
31a′	54% Mn d_{z^2} − 21% CO_{eq} π^* bonding	−0.172	−6.50
	14% Mn $d_{x^2-y^2}$ − 21% CO_{eq} π^* bonding	−0.100	
30a′	38% Mn d_{xy} − Cl p_y bonding	−0.075	−6.68
22a″	43% Mn d_{xz} − 35% Cl p_z bonding	−0.075	−6.69
29a′	7% Mn $d_{x^2-y^2}$ − 61% Cl p_x bonding	0.082	−7.49
	7% Mn p_x − 61% Cl p_x bonding	0.293	
	(b) *fac*-IMn(CO)$_3$(bpy)		
	Unoccupied Orbitals		
35a′	35% Mn $d_{x^2-y^2}$ − 18% I p_x antibonding	0.075	−2.68
	4% Mn p_x − 18% I p_x antibonding	0.354	
25a″	33% Mn d_{yz} − 12% bpy σ antibonding	0.165	−2.89
	6% Mn p_z − 12% bpy σ antibonding	−0.302	
24a″	94% bpy π^*		−3.33
34a′	96% bpy π^*		−3.52
33a′	88% bpy π^*		−4.27
	Occupied Orbitals		
23a″	11% Mn d_{xz} − 83% I p_z antibonding	−0.064	−5.36
32a′	8% Mn d_{xy} − 85% I p_y antibonding	−0.064	−5.44
31a′	41% Mn d_{xy} − 8% I p_y bonding	−0.064	−6.42
	3% Mn$d_{x^2-y^2}$ − 20% I p_x bonding	0.075	
	2% Mn p_x − 20% I p_x bonding	0.354	
22a″	59% Mn d_{xz} − 13% I p_z bonding	−0.064	−6.51
	59% Mn d_{xz} − 11% CO_{eq} π^* bonding	0.140	
	59% Mn d_{xz} − 8% CO_{ax} π^* bonding	−0.140	
30a′	58% Mn d_{z^2} − 20% CO_{eq} π^* bonding	−0.172	−6.56
	10% Mn $d_{x^2-y^2}$ − 20% CO_{eq} π^* bonding	−0.100	
29a′	9% Mn $d_{x^2-y^2}$ − 43% I p_x bonding	0.075	−7.07
	8% Mn p_x − 43% I p_x bonding	0.354	
	16% Mn d_{xy} − 3% I p_y bonding	−0.064	
	16% Mn d_{xy} − 10% CO_{eq} π^* bonding	−0.141	

22a″, the bonding counterparts of 32a′ and 23a″, respectively, to the lowest π^* orbital 33a′. Both assignments agree with the CT character of this absorption band. The first assignment is, however, rather unlikely, since the energy difference between transitions to the first and second π^* orbitals of bpy is normally much larger.[23] Moreover, this assignment does not explain the remarkable intensity changes taking place in the absorption spectrum upon variation of X. Figure 4 clearly shows that, going from X = Cl to X = I, the intensity of the second absorption band increases at the expense of that of the first band.

This effect is connected with the changes in orbital composition taking place upon variation of X. The main transitions of the first and second absorption bands originate from orbitals 32a′ and 30a′ (X = Cl) or 31a′ (X = I), respectively. These orbitals are composed of Mn d_{xy} and X p_y orbitals, 32a′ in an antibonding interaction and 30a′ (31a′) in a bonding combination. Going from X = Cl to Br and I, the ionization potentials of the halide p orbitals will decrease. As a result, the lower-lying orbital 30a′ (31a′) will obtain more metal character and the halide orbital will contribute more to 32a′. This effect is clearly evident from the MO calculations. Because of the strong

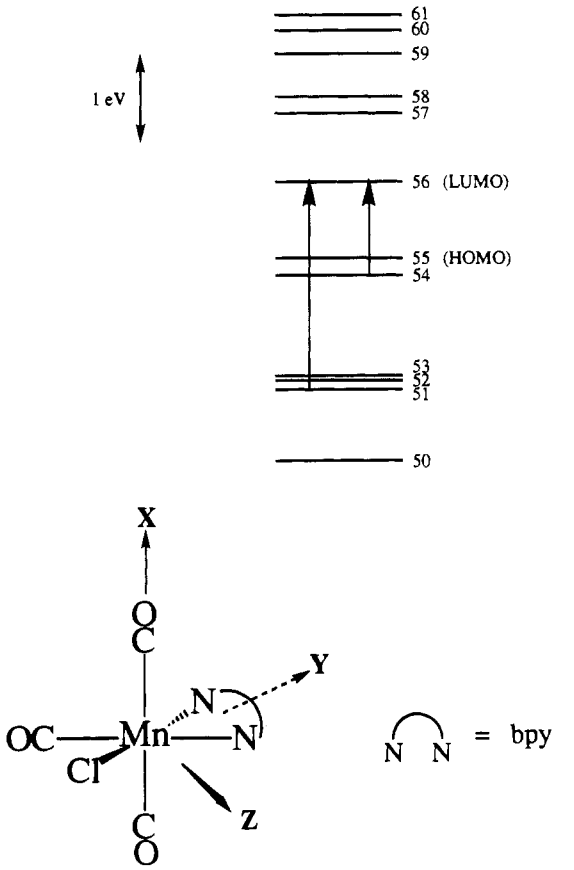

Figure 3. Relevant part of the MO diagram of *mer*-ClMn(CO)$_3$(bpy).

interaction between Mn d_{xy} and 33a′ (vide supra), this metal contribution to 32a′ and 30a′ (31a′) will have a strong influence on the relative intensities of the first and second absorption bands. Going from X = I to X = Cl, the intensity of the first band increases with respect to that of the second one.

This behavior demonstrates that a qualitative relationship exists between the theoretical and spectral data. However, just as the PE spectra (vide supra), the electronic absorption spectra of these complexes show that the results of the MO calculations overemphasize the halide character of the highest filled (metal−halide antibonding) orbitals and the metal character of metal−halide bonding counterparts. Thus, the contribution of Mn d_{xy} to 32a′ is only 8% for X = I, although the intensity of the first absorption band is still rather high. Moreover, the second absorption band is much weaker than the first one in the case of X = Cl, although Mn d_{xy} contributes less to 32a′ (24%) than to 30a′ (38%). A similar effect of the metal contribution on the intensities of the two lowest-energy MLCT bands was recently observed for the closely related complexes XRu(R)-(CO)$_2$(iPr-DAB) (X = halide; R = alkyl).[24] In that case, the relative intensities of the first and second absorption bands were influenced by variation of R. Going from R = Me to Et and iPr the first absorption band of the complexes IRu(R)(CO)$_2$-(iPr-DAB) increased in intensity at the expense of that of the second one. This effect is caused by the increase of electron donation by the R group and the concomitant rise in energy of the metal d orbitals. As a consequence, there is an increase of metal character of the metal−halide antibonding orbitals from which the first CT transitions originate.

We note that taking just the orbital energy differences yields rather poor agreement with the experimental excitation energies.

(23) (a) van Dijk, H. K.; Stufkens, D. J.; Oskam, A. *J. Organomet. Chem.* **1988**, *340*, 227. (b) Stufkens, D. J.; Snoeck, T. L.; Lever, A. B. P. *Inorg. Chem.* **1988**, *27*, 953.

(24) Nieuwenhuis, H. A.; Stufkens, D. J.; Oskam, A. *Inorg. Chem.* **1994**, *33*, 3212.

Table 6. Characters and Energies of the MO's of *mer*-ClMn(CO)$_3$(bpy)

orbital	character	overlap factor	energy/eV
	Unoccupied Orbitals		
61	8% Mn d_{yz} − 5% Cl p_y antibonding	−0.059	−2.36
	8% Mn d_{yz} − 3% Cl p_z antibonding	0.056	
	9% Mn $d_{x^2-y^2}$ − 5% Cl p_y antibonding	−0.003	
	9% Mn $d_{x^2-y^2}$ − 3% Cl p_z antibonding	0.056	
	38% CO_{ax} π^*		
60	77% CO_{ax} π^*		−2.54
59	39% Mn d_{yz} − 13% bpy σ antibonding	0.165	−2.81
	39% Mn d_{yz} − 4% Cl p_z antibonding	0.056	
58	94% bpy π^*		−3.30
57	95% bpy π^*		−3.52
56	91% bpy π^*		−4.29
	Occupied Orbitals		
55	39% Mn d_{z^2} − 13% Cl p_y antibonding	0.061	−5.18
	39% Mn d_{z^2} − 18% Cl p_z antibonding	0.031	
	39% Mn d_{z^2} − 8% CO_{eq} π^* bonding	0.122	
54	14% Mn d_{xy} − 49% Cl p_x antibonding	−0.053	−5.38
	20% Mn d_{xz} − 49% Cl p_x antibonding	0.052	
53	26% Mn d_{xy} − 8% CO_{eq} π^* bonding	−0.101	−6.55
	26% Mn d_{xy} − 14% CO_{ax} π^* bonding	−0.138	
	33% Mn d_{xz} − 8% CO_{eq} π^* bonding	−0.099	
	33% Mn d_{xz} − 14% CO_{ax} π^* bonding	−0.139	
52	19% Mn d_{z^2} − 35% Cl p_y bonding	0.061	−6.64
	19% Mn d_{z^2} − 25% Cl p_z bonding	0.031	
51	20% Mn d_{xy} − 42% Cl p_x bonding	−0.053	−6.73
	13% Mn d_{xz} − 42 Cl p_x bonding	0.052	
	20% Mn d_{xy} − 12% CO_{ax} π^* bonding	−0.138	
	13% Mn d_{xz} − 12% CO_{ax} π^* bonding	−0.139	
50	7% Mn d_{yz} − 33% Cl p_y bonding	−0.059	−7.53
	4% Mn p_y − 33% Cl p_y bonding	0.054	
	4% Mn p_z − 33% Cl p_y bonding	−0.243	
	7% Mn d_{yz} − 37% Cl p_z bonding	0.056	
	4% Mn p_y − 37% Cl p_z bonding	−0.243	
	4% Mn p_z − 37% Cl p_z bonding	0.045	

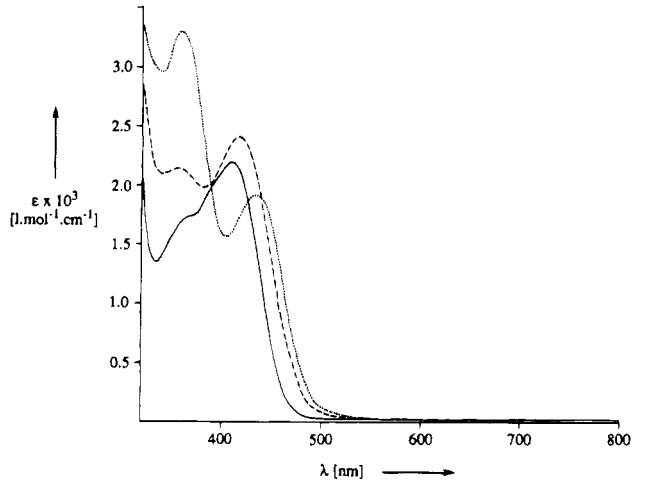

Figure 4. UV/vis spectra of *fac*-ClMn(CO)$_3$(bpy) (—), *fac*-BrMn(CO)$_3$(bpy) (- - -), and *fac*-IMn(CO)$_3$(bpy) (• • •) in 2-MeTHF at 140 K.

We have therefore performed full SCF calculations on the excited states for *fac*-ClMn(CO)$_3$(bpy). The excited singlet states corresponding to the 32a′ → 33a′ and the 30a′ → 33a′ excitations are calculated at 2.31 and 3.55 eV above the ground state, to be compared to the experimental energies 2.95 and 3.45 eV of the first two bands. The agreement is now satisfactory, although the first calculated excitation energy is still rather low compared to experiment. It is interesting to observe that the relaxation effects in the fully self-consistent calculations on the excited states not only improve the calculated excitation energies but also yield relative metal and halide contributions to the 32a′ and 30a′ orbitals that are much better in line with the ones

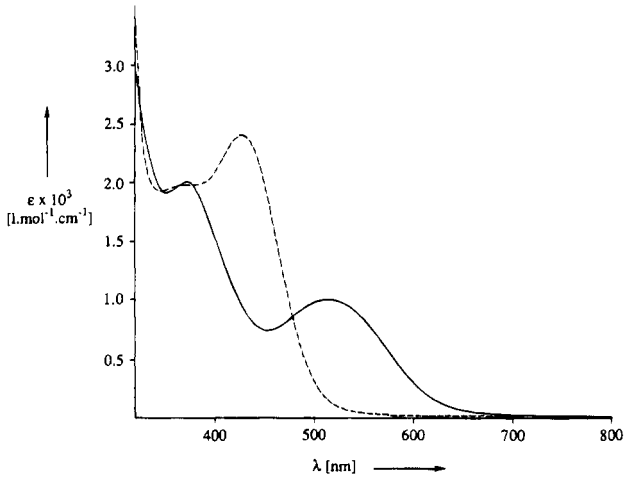

Figure 5. UV/vis spectra of *fac*- (- - -) and *mer*-BrMn(CO)$_3$(bpy) (—) in THF at room temperature (since *mer*-BrMn(CO)$_3$(bpy) is an intermediate in the photochemical reaction depicted in Scheme 1, the spectrum could only be obtained by subtraction).

inferred from experiment. For instance, the metal character of the highest occupied orbital (32a′) increases in the 32a′ → 33a′ excited triplet state to ca. 45% and drops for 30a′ to 15%.

Apart from the CT transitions, the complexes *fac*-XMn(CO)$_3$(bpy) also possess LF transitions at rather low energy. Because of their low intensity, they will be obscured by the intense CT transitions. For the related complexes *fac*-XMn(CO)$_3$(R-DAB) the first LF transition has been observed at 360 nm.[6] In the MO diagrams of the *fac*-complexes under study, the transitions from the close-lying orbitals 30a′, 31a′, and 22a″ to 35a′ or 25a″ can be regarded as such LF transitions.

Because of their thermal instability, the complexes *mer*-XMn(CO)$_3$(bpy) could not be isolated so far. They have been identified and characterized spectroscopically as intermediates in the photoreactions of the corresponding *fac* isomers.[5] The absorption spectrum of *mer*-BrMn(CO)$_3$(bpy), presented in Figure 5, could therefore only be obtained by subtraction, and consequently the extinction coefficients of the band maxima are not very accurate.

Just as for the *fac* isomer, the electronic transition of *mer*-ClMn(CO)$_3$(bpy) which mainly contributes to the intensity of the first absorption band will originate from a MO containing Mn d_{xy}. For the *fac* isomer this is orbital 32a′; the corresponding orbital of the *mer* isomer is 54 (Table 6). Due to the structural change, Mn d_{xy} now interacts with Cl p_x instead of Cl p_y. The electronic transition from orbital 54 will again be directed to the lowest π^* orbital of bpy (56). Just as for the *fac* isomer, the MLCT transition from orbital 51, the bonding counterpart of 54, will mainly be responsible for the intensity of the second absorption band. This orbital is, however, more complex than orbital 30a′ and not only bonding between Mn d_{xy} and Cl p_x. Another difference between the two isomers is the presence of a third orbital (53) in the case of the *mer* isomer, which has an appreciable contribution from Mn d_{xy}. The transition from this orbital toward orbital 56 of bpy will also be allowed, but it does not give rise to a separate absorption band in the absorption spectrum (Figure 5). The second absorption band is much stronger than the first one, and this agrees with the higher contribution of Mn d_{xy} to orbital 51 compared to 54.

The most striking difference between the spectra of the two isomers of BrMn(CO)$_3$(bpy) is the shift to longer wavelength of the first absorption band going from *fac* to *mer*. This effect agrees with the rise in energy going from orbital 32a′ to 54 (Tables 5a and 6). The latter effect is, however, much smaller than the shift of the absorption band.

As already mentioned in the Introduction, the two isomers of $XMn(CO)_3(bpy)$ undergo different primary photoprocesses upon irradiation into their lowest-energy absorption bands. The *fac* isomers lose CO, and the *mer* complexes undergo homolysis of the Mn−X bond, which is a remarkable reaction for a halide complex. The occurrence of a CO-loss reaction is not unexpected, since a similar reaction has been observed for related Mn complexes such as $Ph_3SnMn(CO)_3(\alpha\text{-diimine})$,[25] $(CO)_5Re\text{-}Mn(CO)_3(\alpha\text{-diimine})$,[26] and $CpMn(CO)_2L$ (L = (substituted) pyridine).[27] For the last complexes the efficiency of the photoreaction appeared to depend on the substituent of pyridine and on the energy difference between the MLCT and LF states. This reaction was therefore proposed to proceed from the lowest LF state, after surface crossing from the MLCT states. Quite recently, CASSCF/MRCI calculations of the ground and excited states of *fac*-$HMn(CO)_3$(H-DAB) showed that for this complex the ^{3}MLCT states may be responsible for the CO-loss reaction.[29] A similar mechanism may explain the photochemistry of the *fac*-$XMn(CO)_3(bpy)$ complexes. Going to the *mer* complexes, the first absorption band shifts to longer wavelength (Figure 5) and the lowest excited state decreases in energy with respect to the reactive LF state. As a result, the *mer* isomers do not show release of CO.

The question remains as to why the *mer* complexes undergo homolysis of the Mn−X bond upon irradiation into the lowest-energy absorption band. Such a reaction is not expected, since the electronic transitions take place from the metal−halide π-antibonding orbital 54, which will be accompanied with a strengthening and not a weakening of the Mn−X bond. It is more likely that, just as for the metal−metal-bonded complexes $L_nMM'(CO)_3(\alpha\text{-diimine})$ (L_nM = $(CO)_5Mn$, $(CO)_5Re$, $(CO)_4Co$, Ph_3Sn; M′ = Mn, Re)[2c] and the metal−alkyl-bonded compounds $(R)Re(CO)_3(\alpha\text{-diimine})$,[29] the reaction takes place from the reactive $\sigma_b\pi^*$ state, in which σ_b represents the metal−halide σ-bonding orbital (50) and π^* the lowest unoccupied orbital of bpy (56). Occupation of such a $\sigma_b\pi^*$ state after MLCT excitation has been shown to be responsible for the homolysis of the metal−metal or metal−alkyl bond in the above-mentioned complexes. However, in the case of the *mer* isomer, the $\sigma_b\pi^*$ state may be too high in energy to be occupied after MLCT excitation.

Conclusion

The above results demonstrate that the results of the MO calculations performed on *fac*- and *mer*-$XMn(CO)_3(bpy)$ can be used to determine the character of the electronic transitions of these complexes. The two lowest absorption bands of both isomers are assigned to CT transitions from π-interacting Mn d−X p orbitals to the lowest π^* orbital of bpy. The calculated halide contribution to the highest filled Mn d−X p orbitals seems to be slightly overemphasized. Of course, a proper theoretical evaluation of the relative intensities would have to take into account orbital relaxations in the various excited states.

The difference in primary photoprocess of the *fac* (loss of CO) and *mer* isomers (Mn−X homolysis) may be caused by a lowering of the lowest excited state going from the *fac* to the *mer* isomer. Surface crossing to the lowest LF state will then be prevented in the case of the *mer* isomer, and as a result efficient CO loss cannot occur anymore. The homolysis reaction observed for the *mer* isomer might occur from the excited $\sigma_b\pi^*$ state, just as for the corresponding metal−metal- and metal−alkyl-bonded complexes.

Acknowledgment. Thanks are expressed to the Netherlands Foundation for Chemical Research (SON) and the Netherlands Organization for the Advancement of Pure Research (NWO) for their financial support.

IC930947K

(25) Andréa, R. R.; Stufkens, D. J.; Oskam, A. *Inorg. Chem.* **1989**, *28*, 318.
(26) (a) Kokkes, M. W.; de Lange, W. G. J.; Stufkens, D. J.; Oskam, A. *J. Organomet. Chem.* **1985**, *294*, 59. (b) Kokkes, M. W.; Stufkens, D. J.; Oskam, A. *Inorg. Chem.* **1985**, *24*, 2934. (c) Rossenaar, B. D.; van der Graaf, T.; van Eldik, R.; Langford, C. H.; Stufkens, D. J.; Vlček, A., Jr. *Inorg. Chem.* **1994**, *33*, 2865.
(27) Giordano, P. J.; Wrighton, M. S. *Inorg. Chem.* **1977**, *16*, 160.
(28) Daniel, C. Personal communication.
(29) Rossenaar, B. D.; Kleverlaan, C.; Stufkens, D. J.; Oskam, A. *J. Chem. Soc., Chem. Commun.* **1994**, 63.